Photon focusing, internal diffraction, and surface states in periodic dielectric structures

P. Etchegoin and R. T. Phillips
Cavendish Laboratory, University of Cambridge, Madingley Road, CB3 OHE, Cambridge, United Kingdom
(Received 20 December 1995)

Several analogies between electrons and phonons in semiconductors and electromagnetic waves in periodic dielectric structures are used to demonstrate the existence of (i) surface or edge states at the boundaries between the periodic structure and air, (ii) focusing of the electromagnetic energy emitted by a point source, and (iii) the existence of *internal diffraction* as known for coherent acoustic waves. In addition, the inclusion of dispersion in the optical constants, which is a unique feature of periodic dielectrics and have no equivalent in phonon or electron band structures, is briefly discussed. [S0163-1829(96)10019-9]

I. INTRODUCTION

Since the pioneering work of Yablonovitch[1] a great deal of effort has been put in understanding the properties of electromagnetic waves in periodic dielectric structures (PDS). It has been shown theoretically[2–5] and experimentally[1,6,7] that forbidden gaps exist in PDS and the term *photonic band materials* has been coined accordingly. The literature in the field is vast as the reader may appreciate through some of the papers published in conferences related to or specialized in the subject.[8]

One of the main concerns has been the conditions for the existence of photonic gaps,[4] in particular, the existence of gaps for all possible polarizations of the electromagnetic wave. It very often ensues that gaps for a given polarization do not overlap with gaps for others.[5] The existence and search of forbidden energy regions for arbitrary polarization have been of prime importance in the field. Likewise, different periodic structures show optimum values for the filling fraction of the unit cell in order to open gaps, and these values are different for distinct shapes of the dielectric objects and for different lattices. In this respect, numerical simulation[4] has benefited the selection of possible candidates for observing the desired effects. Last but not least, one major concern has been the possibility of observing electromagnetic localization in disordered dielectrics;[9–14] a subject which would deserve a chapter by itself.

The field has benefited from analogies to and differences from other excitations in solids. The very concept of a gap is an example but more elaborate analogies exist, for instance, the presence of *donor* or *acceptor* states in the gap[15] induced by a defect (as in semiconductors). The search for localization[16] is another example fueled by the familiar examples of Anderson localization for electrons. In these analogies the ultimate differences among the different types of excitations are also highlighted. As an example, the vectorial character of the electromagnetic field is sharply opposed to the scalar nature of electrons leading to different bands for different polarizations. In this particular respect, electromagnetic waves are definitely closer to phonons than electrons. Another difference is the fact that Maxwell's equations have a second-order partial derivative with respect to time, while the Schrödinger equation has only a first partial derivative of t. As a consequence, electrons can have negative energies and become trapped in deep potentials, while the equivalent problem for photons reduces itself to finding eigenvalues of the form $\lambda_i = \omega_i^2/c^2$ which must be >0 if the dielectric function $\epsilon(\omega)$ of the objects forming the lattice is real and positive.

Notwithstanding the major progress in this field, we are convinced that several other analogies with what is known from phonons and electrons can be exploited still for electromagnetic waves in PDS's. In particular, the full consequences of the details of the bands for particular cases have been, in general, overlooked by the search of a reasonable parameter set producing the desired gap. The nature of the wave propagation in these structures is fascinating by itself and leads to very interesting phenomena already known for phonons as we shall show later. Furthermore, not all analogies with electrons have been exploited so far. We shall show the example of *surface states at the boundaries* obtained from the bulk band structure, in complete equivalence with what is known for electrons in semiconductors. Of particular interest are the existence of *pure surface states*, i.e., solutions with energies in the forbidden gap. We show that these solutions exist through a calculation for a particular example and compare our method of calculation with previously reported supercell results.[17]

The paper is organized as follows: Sec. II gives a brief introduction to the method of calculation and the band structures for the examples we shall use. Section III presents the calculation and underlying concepts for the surface states. Section IV shows explicitly how the existence of bands can produce focused emission by a point source and the phenomenon of *internal diffraction* as known for acoustic phonons. Section V presents the possibility of including dispersion in the dielectrics, a feature which has no counterpart for phonons or electrons. Finally, Sec. VI underscores a few analogies between long-wavelength electromagnetic waves and the theory of elasticity for sound waves. In Sec. VI a few final remarks are given.

II. THEORETICAL OVERVIEW

We deal with two-dimensional (2D) periodic dielectric structures for simplicity. Furthermore we restrict ourselves to propagation perpendicular to the rods. Since we deal with a periodic structure Bloch's theorem applies. We know the

electric $\vec{E}(\vec{k},\omega)$ [or magnetic $\vec{H}(\vec{k},\omega)$] field of the propagating wave can be expressed as

$$\vec{E}(\vec{k},\omega)=\sum_{\vec{G}} A(\vec{G},\vec{k})e^{i(\vec{k}+\vec{G})\cdot\vec{r}}, \tag{1}$$

where $\vec{r}=x\hat{i}+y\hat{j}$ is a vector in the plane perpendicular to the rods and $\vec{G}$ are the reciprocal-lattice vectors of the selected lattice. By replacing (1) into Maxwell's equations[4,5] the propagation for polarization perpendicular to the rods $[\vec{E}(\vec{k},\omega)\perp z\hat{k}]$ is reduced to the eigenvalue problem

$$\sum_{\vec{G}'} (\vec{k}+\vec{G})\cdot(\vec{k}+\vec{G}')\kappa(\vec{G}-\vec{G}')A(\vec{G}',\vec{k})=\frac{\omega^2}{c^2}A(\vec{G},\vec{k}), \tag{2}$$

where $A(\vec{G},\vec{k})$ are the Fourier components of $\vec{H}(\vec{k},\omega)$ and $\kappa(\vec{G}-\vec{G}')$ are the Fourier expansion coefficients of the inverse of the position-dependent dielectric function $\epsilon(\vec{r})$ (considered here as dispersionless and >0). If $\vec{E}(\vec{k},\omega)$ is parallel to the rods the eigenmodes are obtained from[4,5]

$$\sum_{\vec{G}'} (\vec{k}+\vec{G}')^2\kappa(\vec{G}-\vec{G}')A(\vec{G}',\vec{k})=\frac{\omega^2}{c^2}A(\vec{G},\vec{k}), \tag{3}$$

where $A(\vec{G},\vec{k})$, in this case, are the Fourier components of the electric field. Solving the electromagnetic band structure through (2–3) is equivalent to solving an electronic band structure by the pseudopotential method.[18] The main differences with the electronic case are (i) the existence of different band structures according to polarization and (ii) the fact that empirical pseudopotentials are relatively smooth functions of $\vec{G}$, while periodic dielectric structures have sharp dielectric discontinuities and several Fourier coefficients $\kappa(\vec{G}-\vec{G}')$ are needed in the expansion. Consequently, electronic band structures in semiconductors (with only three Fourier coefficients for the pseudopotential[18]) can be calculated with a plane-wave basis of $\sim 60-90$ waves, while (2–3) need normally a basis of size >200.

We shall use two examples in this paper with filling fractions f taken from Ref. 4 to optimize the opening of a gap. The first is one is a 2D triangular lattice filled with circular rods of dielectric constant $\epsilon=5$. The background is assumed to be air ($\epsilon=1$). The filling fraction (defined as the area occupied by the circular rods per cell, normalized by the area of the cell) is $f=0.169$. The electromagnetic band structure for polarization parallel to the rods is shown in Fig. 1(a) for the principal symmetry directions (shown also in the figure). These bands have been calculated with a basis of 499 plane waves. In Fig. 1(b) we show the density of states (DOS) of electromagnetic modes calculated through a random sampling of 10^4 $\vec{k}$ vectors in the 1/12th-irreducible part of the first Brillouin zone (BZ) between Γ, X, and Λ. Energies are reduced to dimensionless quantities by the factor $\tilde{\omega}\rightarrow\omega(2\pi a/c)$, where a is the lattice parameter and c the speed of light. The following features should be noticed for the forthcoming discussion: (i) the existence of a gap around $\tilde{\omega}\sim 0.45$ [see also Fig. 1(b)]; (ii) the presence of an *acoustic-like* branch below the gap (with $\tilde{\omega}\propto k$ close to Γ) and (iii) the existence of relatively flat bands above the gap (also seen as sharp singularities in the DOS). Note also that the gap is defined between the maximum energy of the *acoustic* branch at Λ and the minimum of the bands above the gap (hereafter conduction bands in analogy with semiconductors) at X. In the language of semiconductors this would be a structure with an indirect gap.

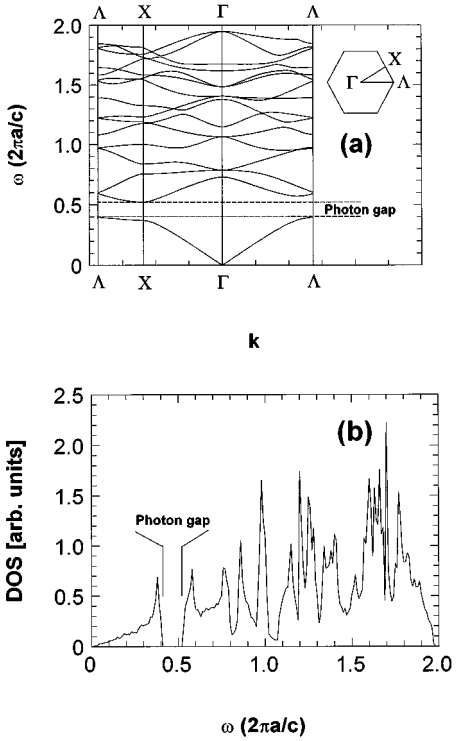

FIG. 1. (a) Electromagnetic band structure (with 499 plane waves) for a triangular lattice of dielectric rods with $\epsilon=5$ in air ($\epsilon=1$). The filling factor of the structure is $f=0.169$ and the bands correspond to polarization parallel to the rods. The hexagonal BZ and the principal symmetry directions are also given; (b) DOS as obtained from a random sampling of 10^4 $\vec{k}$'s in the region limited by Γ, X, and Λ.

The second example we use is shown in Figs. 2(a) and 2(b). The lattice is again triangular with cylindical rods but the dielectric function of the rods is now $\epsilon=14$ with a filling fraction of $f=0.431$.[4] The band structure, however, corresponds to polarization perpendicular to the rods. The same features of the first example can be observed here. The DOS has been calculated as in Fig. 1(a). Note also that in both Figs. 1(a) and 2(a) the *direct* gap at Λ is slightly larger than the one at X.

III. SURFACE STATES

Having presented the electromagnetic band structures for two infinite PDS's in the previous sections we discuss here the existence of surface states as obtained from the bulk band structure. The aim of this section is to show a specific example of surface states and discuss briefly their implications.

Every real implementation of a PDS is necessarily finite. The existence of surfaces in the structure allows the presence of solutions which are not directly contemplated in (2–3) if

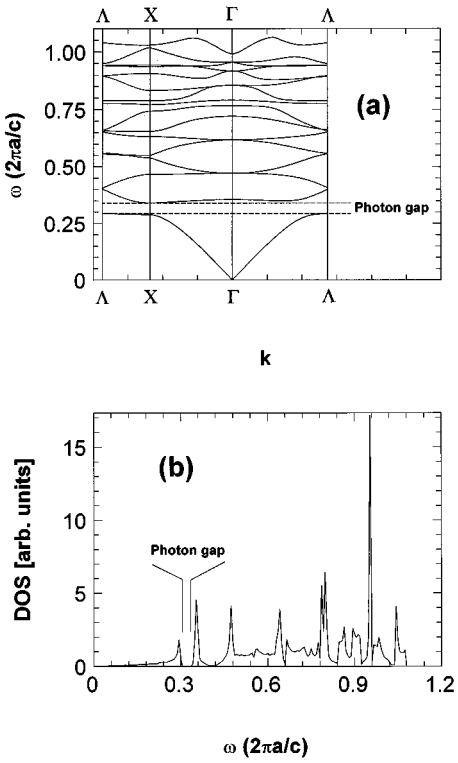

FIG. 2. Same as Figs. 1(a) and 1(b) but for dielectric rods of $\epsilon=14$ in air and polarization perpendicular to the rods; (b) DOS calculated as in Fig. 1(b).

$\vec{k}$ is real. In fact, Bloch's theorem vouches for solutions of the form (1) but does not restrict $\vec{k}$ to be real. The latter comes as an aftermath to the fact that only nondivergent solutions for the fields are physically acceptable. If $\vec{k}$ is allowed to have an imaginary component in (1) the field will irremediably diverge in an infinite lattice. This constraint is removed if a surface is introduced and this is a standard textbook example of surface states.[19] Let us briefly review how these states are formed in the nearly-free-electron model. Take a 1D weakly periodic potential as $V(x)=U_0\exp(iGx)$. This opens (in first order) only one gap at the boundary of the first BZ. The two wave functions at the gap can be expressed as $\Psi\sim C_1\exp(ikx)+C_2\exp[i(k-G)x]$ where $C_{1,2}$ come from the Hamiltonian

$$\begin{pmatrix}\lambda_1 & U_0\\ U_0 & \lambda_2\end{pmatrix}\begin{pmatrix}C_1\\ C_2\end{pmatrix}=E\begin{pmatrix}C_1\\ C_2\end{pmatrix} \tag{4}$$

with $\lambda_1=\hbar^2k^2/2m$, $\lambda_2=\hbar^2(k-G)^2/2m$ and eigenvalues $E=\frac{1}{2}(\lambda_1+\lambda_2)\pm\sqrt{\frac{1}{4}(\lambda_2-\lambda_1)^2+U_0^2}$. Expressing wave vectors with respect to the zone boundary $g=(G/2-k)$ and energies E with respect to the center of the gap we obtain $\lambda_g=\sqrt{E^2-U_0^2}$ with $\lambda_g=\hbar^2g^2/2m$. Two cases are distinguished: (i) $|E|>U_0$ with real values of $(G/2-k)$ and (ii) $|E|<U_0$ with imaginary λ_g, i.e., imaginary wave vectors. These solutions decay exponentially inside the solid and can be matched to evanescent waves into the vacuum to become surface states. In fact, these solutions are an *analytic continuation* of the band structure through the gap. Details of the matching rely on the exact position chosen for the surface relative to the phase of the modulation potential $U_0\exp(iGx)$. This approach has been used very successfully for semiconductors and reports for GaAs, Si, and Ge can be found as early as 1966 (Ref. 20) in calculations using the $\vec{k}\cdot\vec{p}$ method for the bulk electronic states. In a solid, surface states can be calculated for the different inequivalent surfaces of the structure. In GaAs and the like, surface eigenstates with imaginary $\vec{k}$ are normally calculated for [111], [1$\bar{1}$0], and [001] surfaces. For a 2D triangular lattice there are two different inequivalent surfaces shown in Fig. 3 that cut the structure through lattice sites (atomic positions in the case of electrons). We calculate the electromagnetic surface states for these two surfaces for polarization perpendicular to the rods.

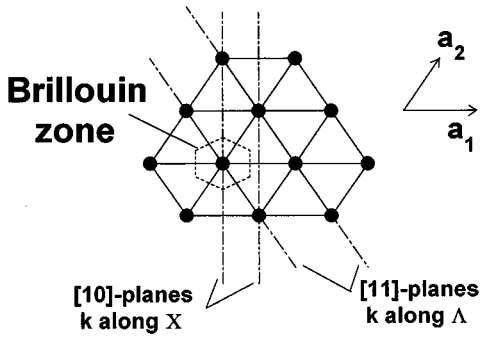

FIG. 3. Triangular lattice and lattice planes along [10] and [11]. Families of lattice planes are normal to $\vec{k}$ vectors along principal symmetry directions. Planes along [10] are normal to $\vec{k}$'s along X, while those along [11] are $\perp$ to $\vec{k}$'s along Λ. The hexagonal BZ of the triangular lattice is shown schematically around one lattice point.

Normally, as in the 1D example for surface states shown previously, solutions with imaginary $\vec{k}$ will show up as analytic continuations connecting neighboring roots for real $\vec{k}$ at a given point in the BZ.[20] As we shall show later, these analytic continuations may interact and cross with each other and connect eventually the solutions for real $\vec{k}$ at ω with their mirror images at $-\omega$ which are, in turn, analytic continuations in the $\omega<0$ plane. The best way to obtain solutions in the gap, for example, is to start in those points of the BZ that have eigenenergies for real $\vec{k}$ on both sides and close to the gap in question. A situation like the one depicted in the 1D example given above can be, therefore, expected in which the analytic continuation crosses the gap and produces surface states with no energy overlap with respect to the bulk bands. An additional characteristic of the surface states obtained by these analytic continuations is that they formally regard the surface as a sharp, featureless, flat interface in the matching with external solutions. The latter is certainly not a limitation for 1D layered media[21–25] but is not formally correct in 2D or 3D PDS's where surfaces are not flat planes but have their own topology. Accordingly, roots with very large $\mathrm{Im}(\vec{k})$ (i.e., with fields penetrating less than a single layer) are not to be taken as *good* solutions to match with waves into the vacuum, in the sense that the field pattern is nonnegligible only in the region where the original approxima-

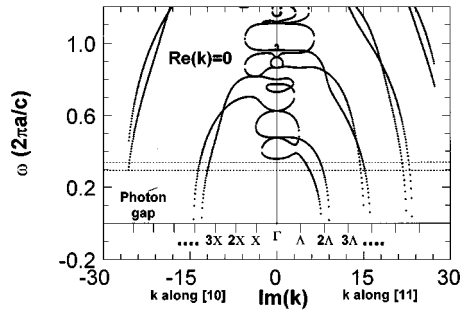

FIG. 4. Surface states at Γ calculated with 271 plane waves. Both branches of the analytic continuations along X and Γ are joined at Γ. These states with $\mathrm{Re}(\vec{k})=0$ represent pure exponential deacays of the fields inside the structure (see text for details).

tion of a flat, sharp, interface is not valid. Another possibility to study modes at the surface is to solve a supercell formed by layers separated by air, in exact analogy to what is done for electrons.[17] The latter is a more sophisticated approach that avoids the problem of matching and bequeaths directly all solutions which can be classified as[17] (i) extended in both the crystal and air, (ii) decaying in air and the crystal, (iii) extended in air and decaying in the crystal, and, (iv) decaying in both air and the crystal. These solutions treat the surface details correctly. The price to be paid is to work with supercells which have to be defined for each direction of interest. In addition, solutions with very long penetration depths (larger than the supercell size) are not properly treated. To some extent, this method is complementary to ours which treats better those solutions with large penetrations into the bulk. Moreover, the method presented here uses the very same band structure of the bulk and does not require additional computational effort in building the supercells. It also provides solutions along directions other than the principal for which a supercell method may prove to be impossible and gives a quick answer to penetration depths in the gaps along different directions.

In Fig. 4 we show the surface states at Γ [i.e., Re $(\vec{k})=0$] for the bands in Fig. 2(a). We plot two cases in Fig. 4: (i) $\mathrm{Im}(\vec{k})\|[10]$ and (ii) $\mathrm{Im}(\vec{k})\|[11]$. Since $\mathrm{Re}(\vec{k})=0$, both cases are branches of the same analytic function and can be therefore joined at Γ. The calculation is perfomed with a basis of 271 plane waves. These solutions represent states that are pure exponential decays of the field inside the structure. According to the previous discussion, states across the gap at $\tilde{\omega}\sim 0.32$ are not expected for small $\mathrm{Im}(\vec{k})$, since none of the states at Γ define this gap. After some crossings and anticrossings the analytic continuations of the solutions at Γ show several branches pointing downwards that would meet the mirrored solutions in the plane $\omega<0$ if we made the analytic continuations there. Some of these branches cross the gap but only for large values of $\mathrm{Im}(\vec{k})$. There are, however, plenty of solutions with small $\mathrm{Im}(\vec{k})$ in the *conduction band*. These solutions penetrate the structure several lattice constants as a pure exponential decay. It is worth noting that there is a fundamental difference in this respect with the electronic case. Although solutions that overlap with the conduction and valence band in semiconductors are obtained as in here, comparison with an experimental determination of

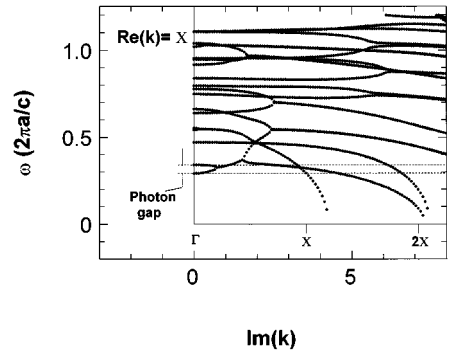

FIG. 5. Surface states at X calculated as in Fig. 4 but with $\mathrm{Re}(\vec{k})=X$. Note the existence of solutions in the gap for $\mathrm{Im}(\vec{k})<|X|$. These solutions have both, an exponential decay and a modulation given by $\mathrm{Re}(\vec{k})$. The field pattern for midgap energy is shown in Fig. 7.

these states cannot ignore the strong scattering electrons suffer with the bulk bands which are degenerate with them. In the case of electromagnetic waves this limitation is removed and solutions at the surface calculated by this method are expected to be more reliable. Photons do not interact with each other in linear media and the existence of bulk states with the same or similar energies to these surface states do not perturb or scatter them by any means.

A more interesting situation results when considering surface states at X and Λ as shown in Figs. 5 and 6. In these figures we set $\mathrm{Re}(\vec{k})$ to be either at X or at Λ and we allow $\mathrm{Im}(\vec{k})$ to be $\neq 0$ to find the analytic continuations of the bands around those points in the BZ. Figure 5 shows that the two solutions above and below the gap at $\mathrm{Im}(\vec{k})=0$ are attracted to each other and join in the forbidden gap of the bulk at a value of $\mathrm{Im}(\vec{k})\ll|X|$, i.e., there are solutions in the gap which expand over several lattice constants in real space. Figure 6 shows the equivalent calculation for a [11] surface. If we take the midgap energy as a reference, and we find the solution with the smallest $\mathrm{Im}(\vec{k})$ for the surface states at Λ

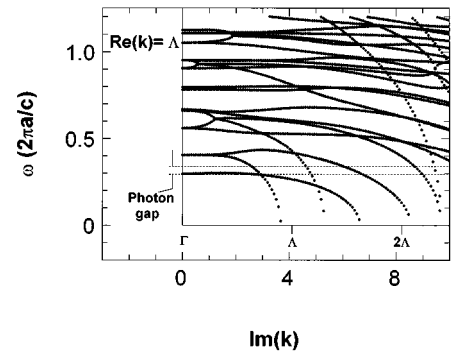

FIG. 6. Surface states at Λ [i.e., $\mathrm{Re}(\vec{k})=\Lambda$] calculated as in Figs. 4 and 5. There is a crossing of one branch through the gap at $\mathrm{Im}(\vec{k})$ smaller than the zone boundary along this direction (as in Fig. 5). Note that the solution at midgap energy with the smallest $\mathrm{Im}(\vec{k})$ implies a shorter penetration in the structure than than for a [10] surface in Fig. 5 (see text for details).

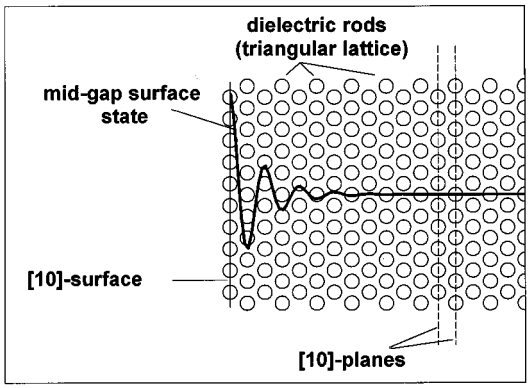

FIG. 7. Field distribution for the surface state at midgap energy (polarization $\perp$ to the rods) on a [10] surface taken from Fig. 5. The triangular lattice of circular rods is plotted for comparison and the [10] planes indicated. Note that this solution penetrates roughly 10 lattice planes and that this is about four times the penetration depth at the same energy for a [11] surface (see Fig. 6).

and X, we note that electromagnetic waves have a larger penetration depth inside the bulk for a [10] surface than for a [11] one. The branch starting from the solution immediately above the gap at Λ in Fig. 6 decreases and crosses the midgap energy at $\mathrm{Im}(\vec{k}) \sim 0.75|\Lambda|$. By comparing the latter with the solution of smallest $\mathrm{Im}(\vec{k})$ for the same energy at X in Fig. 5 we find that electromagnetic waves penetrate $\sim$four times more on a [10] surface than on a [11] one. The field pattern for the midgap solution with the smallest $\mathrm{Im}(\vec{k})$ on a [10] surface is plotted in Fig. 7. This solution has, beside the exponential decay, an oscillatory modulation produced by $\mathrm{Re}(\vec{k}) = |X|$. Note that the general shape of the analytic continuations in Figs. 4–6 convey the same impression of the surface states for electrons in semiconductors calculated in Ref. 20.

The existence of surface states is a natural consequence of *any* excitation in a periodic structure and are an artless outcome of Bloch's theorem, albeit they are normally ignored except when the physics of the interface becomes an important part of the problem. Roots of the bulk band structure with imaginary $\vec{k}$ are an unavoidable aspect of many practical aspects of the physics of the interfaces in PDS's. Examples would include the expansion of a field in a defect or impurity close to the surface[26] but, more importantly perhaps, the very process of reflection of electromagnetic waves. Suppose the following situation: an electromagnetic wave impinges from the outside onto a PDS, along a given symmetry direction, with an energy ω lying in the gap. We know that the wave is neither propagated in the forward direction nor absorbed, since dissipative (imaginary) components were not included in the dielectric functions of the rods and, therefore, energy is preserved. The latter means that the wave is going to be reflected and we ask ourselves how the field at the interface looks in the reflection process. It is through the coupling to these evanescent waves that the reflection process takes place and, from that point of view, they constitute an important part of the understanding of how we can couple to these structures from the outside.[17] Needless to say, the physics of the electromagnetic modes at the interface of these structures is far from being exhausted by the simple example given here. We shall come back briefly to some of these aspects in Sec. VI.

IV. PHOTON FOCUSING AND INTERNAL DIFFRACTION

We shall now turn briefly to another aspect of wave propagation in these structures. We show here the direct consequence of the existence of bands onto the emsission produced by a point source and its relation with known phenomena for phonons.

In anisotropic media energy does not flow in the same direction of $\vec{k}$. When excitations are represented by bands labeled by $\vec{k}$ with a given dispersion $\omega(\vec{k})$, energy flows in the direction of the group velocity $\vec{v} = \vec{\nabla} \cdot \omega(\vec{k})$. In fact, it can be shown formally that $\vec{v}$, obtained as a gradient of $\omega(\vec{k})$, coincides with the direction of the Pointing vector $\vec{S} \propto \vec{E} \times \vec{H}$ for electromagnetic waves.[27] For a given fixed energy we can define two surfaces: (i) the constant energy (or slowness) surface, obtained directly from the band structure as the intersection of the bands with a given energy abscissa and, (ii) the wave surface, formed by the locus of all possible group velocities. The wave surface represents the wave front that would emerge from a point source had it emitted a pulse of a few cycles at ω. In order to fix ideas we show a specific example for the bands shown in Fig. 1(a). Figure 8(a) shows two slowness surfaces for the band structure in Fig. 1(a) at two different values of the reduced energy $\tilde{\omega} =$ 0.365 and 0.76. The curve at $\tilde{\omega} = 0.365$ cuts the *acoustic branch* almost at the zone boundary of the first BZ and has a small (barely visible) anisotropy between the values along Λ and X (the surface is $\sim$1.5% larger along X). The curve for $\tilde{\omega} = 0.76$ is, however, very anisotropic between Λ and X and comes only from the second *conduction band* in Fig. 1(a). The reason why we have chosen these two particular cases will become clear soon. In Fig. 8(b) we show the calculated wave surfaces for these two cases, by numerically evaluating $\vec{v}$ from the band structure on the slowness surface. From Fig. 8(b) we see that the wave surface for $\tilde{\omega} = 0.365$ is anisotropic and shows that electromagnetic waves emitted by a point source will travel faster along Λ than along X at this particular energy. Moreover, *the fact that the wave surface is anisotropic produces focusing of the emission in complete analogy with the phenomenon of (acoustic) phonon focusing.*[28] Even when the source may send forth an isotropic distribution of wave vectors, the corresponding distribution of *group velocity vectors* $\vec{v}$ will be anisotropic and consequently the photon emission. An additional important feature is that the wave surface for $\tilde{\omega} = 0.365$ is single valued, in other words, it has no folds and for a given direction of $\vec{v}$ there is only one crossing with the surface. As a consequence, for a particular direction defined by a vector $\vec{r}$ from the source, there is only *one* group velocity vector $\vec{v}$ parallel to $\vec{r}$ contributing to the energy flux in that direction and therefore only *one* wave vector $\vec{k}$ (not necessarily in the same direction). Accordingly, no interference among different $\vec{k}$'s occurs. A very different situation comes about for $\tilde{\omega} = 0.76$ as shown in Fig. 8(b). The wave surface for this case [obtained from the slowness sur-

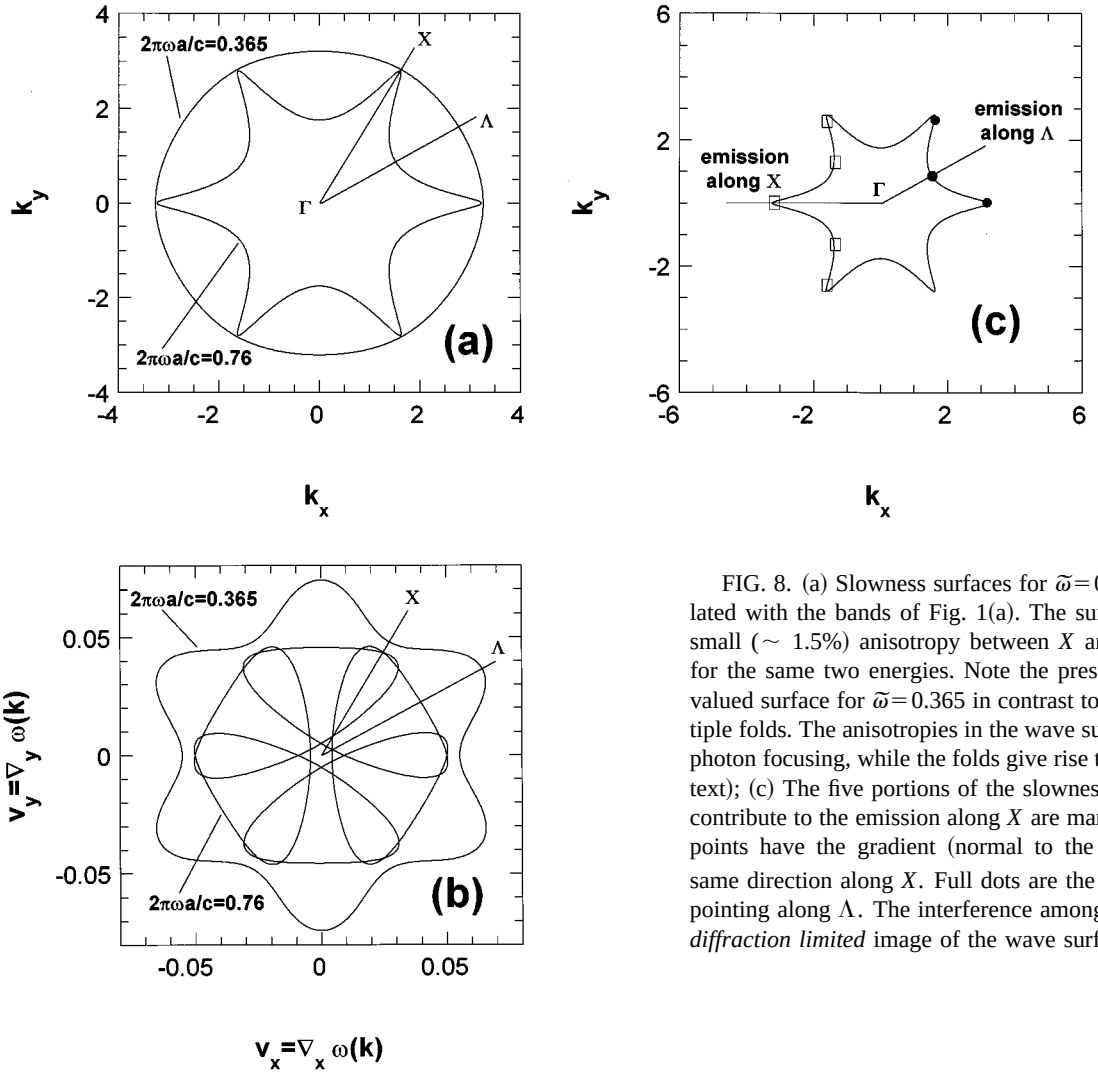

FIG. 8. (a) Slowness surfaces for $\tilde{\omega}=0.365$ and $\tilde{\omega}=0.76$ calculated with the bands of Fig. 1(a). The surface for $\tilde{\omega}=0.365$ has a small ($\sim$ 1.5%) anisotropy between X and Λ; (b) Wave surfaces for the same two energies. Note the presence of a smooth single-valued surface for $\tilde{\omega}=0.365$ in contrast to $\tilde{\omega}=0.76$ which has multiple folds. The anisotropies in the wave surfaces are responsible for photon focusing, while the folds give rise to internal diffraction (see text); (c) The five portions of the slowness surface at $\tilde{\omega}=0.76$ that contribute to the emission along X are marked with a square. These points have the gradient (normal to the surface) pointing in the same direction along X. Full dots are the three $\vec{k}$'s with a gradient pointing along Λ. The interference among these modes produces a *diffraction limited* image of the wave surface.

face in Fig. 8(a)] shows a complex structure of folds. Note, in addition, that along $\Gamma-\Lambda$ and $\Gamma-X$ the second *conduction band* in Fig. 1(a) has a negative slope and, accordingly, energy flows in this case in the direction *opposite* to $\vec{k}$. If we take the emissions along Λ and X we note that the wave surface is cut in three and five places, respectively. Indeed, it is very easy to identify these contributions as shown in Fig. 8(c), where we show the slowness surface for $\tilde{\omega}=0.765$ with those $\vec{k}$'s on it that have the same direction for the gradient (normal to the surface) pointing towards Λ or X. In the case of emission along X two pairs of points shown in Fig. 8(c) are doubly degenerate (i.e. same direction and modulus for the gradient) while one is single degenerate (the intersection of the slowness surface right along X). These constitute the five crossings of the wave surface in Fig. 8(c). Along Λ, two points on the slowness surface are degenerate and one has a different value for the modulus of $\vec{v}$, these are, respectively, the three crossings along Λ of the wave surface in Fig. 8(b). This new situation implies that energy emitted along a given direction will come from several different $\vec{v}$'s and, consequently, from different $\vec{k}$'s, displaying and interference pattern. This is called *internal diffraction* and was predicted by Maris[29] for acoustic-phonon emission in those case where the wave surface has folds as in here. It is sometimes claimed that this effect has no optical analog.[28,30]

In Figs. 9 and 10 we show an explicit calculation of the photon emission by a point source at these two energies. The reason for using the bands with polarization parallel to the rods in this example is that the different electric fields, diffracted along different directions, add up like scalars. In Fig. 9 we show the coherent and incoherent emission at a fixed distance from a point source as a function of angle. The principal symmetry directions are indicated in the figure. Since the wave front has no folds in this case, only one $\vec{v}$ and one $\vec{k}$ contributes to the emission for a given angle and therefore there is no interference among them. The energy is, however, strongly focused along limited solid angles $d\Omega$. In Fig. 10 a very different situation arises between the coherent and incoherent emissions. In addition to a strong focusing of the emission along X [Fig. 10(a)] the coherent case shows a complex interference pattern coming from the simultaneous action of modes with different $\vec{k}$'s but the same group velocity directions. One of the lobes along X is shown in detail in Fig. 10(b) for both coherent and incoherent emission. Actually, the coherent emission represents a *diffraction limited image of the wave surface* in complete analogy with acoustic

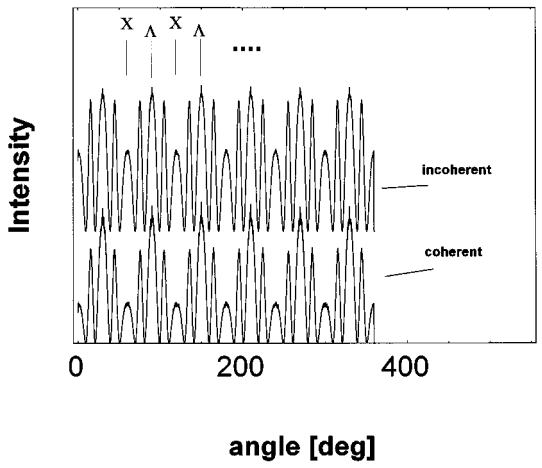

FIG. 9. Coherent and incoherent emission by a point source at $\tilde{\omega}=0.365$ as a function of angle. The intensity pattern is calculated at a constant radial distance from the source of 100 lattice constants. Principal symmetry directions are indicated accordingly. Since the wave surface is single valued no internal diffraction takes place and both cases look essentially the same. The emission is however strongly focused along certain directions. Minima in these curves are very close to zero. The curves have been shifted vertically for clarity.

phonons.[28–30] Note also the existence of sharp singularities in the incoherent emission. These singularities can arise if the *direction* of the group velocity $\vec{v}=\vec{\nabla}\cdot\omega(\vec{k})$ is stationary for one mode with respect to a small variation in $\vec{k}$,[29] in other words, if the wave surface moves *radially* instead of *tangentially*. This is actually the case on both sides of the lobes along X of the wave surface for $\tilde{\omega}=0.76$ in Fig. 8(b) and gives rise to a divergence (infinite emission) along certain directions. This phenomenon is also known for acoustic phonons[28] and is linked to the more general phenomenon of phonon focusing. It is worth noting that internal diffraction

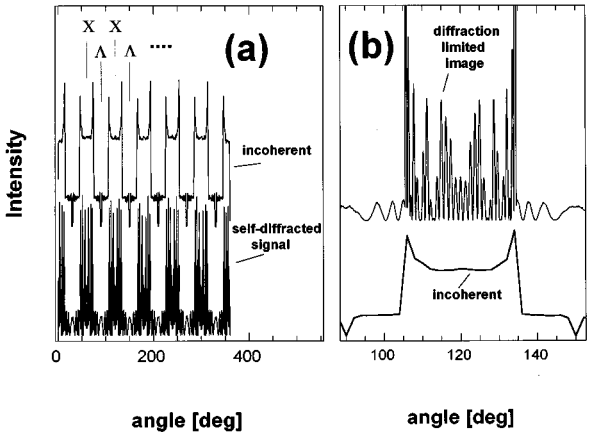

FIG. 10. (a) same as Fig. 9 but for $\tilde{\omega}=0.76$. The existence of folds in the wave surface produces a very different pattern for coherent and incoherent waves. The coherent emission forms a diffraction limited image of the wave surface as shown in (b). In addition, sharp singularities coming from the *directions of infinite intensity* can be seen in the incoherent pattern (see text for details).

does not exist in crystal optics of uni- or biaxial crytals. The electromagnetic modes in a crystal with dielectric tensor $\hat{\epsilon}_{ij}$ are obtained from Fresnel equations

$$k^2\vec{s}\times(\vec{s}\times\vec{a}_\omega)+\frac{\omega^2}{c^2}\hat{\epsilon}\cdot\vec{a}_\omega=0, \tag{5}$$

where $\vec{s}=\vec{k}/|k|$, and $\vec{a}_\omega$ a unit vector in the direction of the electric field. Let us express all the coordinates in the *principal axes basis* where $\hat{\epsilon}_{ij}$ is diagonal and take the example of both $\vec{k}$ and $\vec{a}_\omega$ in the *x-y* plane. It is not difficult to show that the dispersion relation in this case is $\omega=c\sqrt{k_x^2/\epsilon_{yy}+k_y^2/\epsilon_{xx}}$, i.e., the slowness surfaces for any ω is an ellipse. Therefore, emission by a point source in a crystal like this can be focused but the wave surface has neither folds nor singularities producing directions of infinite emission. These are two peculiarities added by the PDS. In fact, the *focusing* effect is very mild in birefringent crystals and is normally refered to simply as *anisotropy of the wave surface*. A situation with a contrast among different solid angles of almost 100% as in Figs. 9 and 10 cannot normally be obtained.

Had we observed the emission of a point source on a surface (instead of at a fixed radial distance as in Figs. 9 and 10) then the intensity pattern is a projection of the wave surface onto the surface in question. This image is again diffraction limited if folds in the wave front exist. Extensions to 3D of all these phenomena are straightforward.

In conclusion, we showed in this section that the phenomena of phonon focusing, directions of infinite emission and internal diffraction[28–30] have their direct analogs for electromagnetic waves in PDS's. In the case of phonons these phenomena can be observed under special conditions. Limiting factors are temperature and different scattering mechanism of the coherently generated phonons. Actually, *focusing and coherent interference is a natural consequence of any excitation represented by anisotropic bands*. The reason why these phenomena are not relevant for electrons, for example, is that scattering times are very short and the possibilities of observing collisionless coherent transport over macroscopic distances (and spatial interference among different wave functions) are very limited if (hot) electrons are expected to be distributed among different bands and valleys and remain there for long times. To some extent the same can be said for phonons, except for acoustic modes at very low temperatures in crystals with anisotropic slowness surfaces (like silicon[28]). All these limitations do not exist for electromagnetic waves which are long lived, can have special coherence attributes and are not thermally scattered. In addition, several different types of sources and detectors can be used. These advantages would put PDS's in a privileged position to study coherent wave propagation in complex structures.

V. PERIODIC DIELECTRICS WITH DISPERSION

So far, only examples in which the dielectrics are dispersionless have been considered. This is due to its conceptual simplicity but also because all practical implementations of PDS's to date fall in this category. It is however interesting to explore the possible consequences of dispersion in the dielectrics on the overall picture of the band structure. To

this end, let us review briefly the consequences of including dispersion in $\epsilon(\vec{r})$. If ϵ depends on ω so does $\kappa(\vec{G})$ through

$$\kappa(\vec{G},\omega)=\sum_{\vec{G}} \frac{1}{\epsilon(\vec{r},\omega)} e^{-i\vec{G}\cdot\vec{r}}. \tag{6}$$

Let us take the example of bands for polarization perpendicular to the rods given by (2). We write the eigenvalue problem (2) in a slightly more formal manner as $\hat{M}_{ij}(\vec{k},\omega)A_j=\lambda A_i$, where A_i are the Fourier components of the field, $\hat{M}_{ij}(\vec{k},\omega)=(\vec{k}+\vec{G}_i)\cdot(\vec{k}+\vec{G}_j)\times\kappa(\vec{G}_i-\vec{G}_j,\omega)$, and $\lambda=\omega^2/c^2$. In the most general case, the ω dependence cannot be factorized from the matrix $M_{ij}(\vec{k},\omega)$ and, therefore, the problem of finding suitable solutions for ω reduces itself to work out the roots of a nonlinear function of ω (containing transcendental functions) obtained from a $n\times n$ determinant, being n the size of the plane-wave basis in use. This problem represents a formidable task. As mentioned in the Introduction, solving Eqs. (2–3) is equivalent to an electronic band-structure calculation by means of the pseudopotential method. The Fourier components $\kappa(\vec{G})$ play in this analogy the role of the pseudopotential coefficients. Allowing an ω dependence in $\kappa(\vec{G})$ would be equivalent to having *time-dependent pseupotentials* for the electrons. In fact, any calculation of electron-phonon interaction implies a time-dependent pseudopotential. Phonons *modulate* the atomic positions and, consequently, the total pseudopotential of the structure is modulated at the frequency of the phonons and produces scattering of the electronic states. The latter is however an example in which the time dependence of the pseudopotential can be treated as a perturbation of the *frozen* band structure. Our case here is equivalent to a time-dependent pseudopotential calculation which cannot be treated perturbately and, accordingly, has no direct analog for electrons. There are of course a few examples for electrons in which the perturbation cannot be treated perturbately and a new exitation is created. Representatives are exciton-polaritons and also resonant interactions with phonons obtained in special cases (magnetic fields, for example). These affect, however, only a limited number of states in the band structure (those in resonance with the excitation).

The solutions of the nonlinear transcendental equation for ω produced by the determinant $|\hat{M}_{ij}(\vec{k},\omega)-(\omega^2/c^2)\delta_{ij}|$ can transform the discrete spectrum of eigenvalues of the original bands into a mixture of continous and discrete energy bands for a given $\vec{k}$ depending on several factors; among them: the type of dispersion selected for the dielectrics, the dispersion of the background medium, the proximity to resonance, etc. There are a few trivial examples in which the dispersion can be factorized from $M_{ij}(\vec{k},\omega)$ and the problem can be solved by avoiding the nonlinear determinant. Even here, a numerical solution of one transcendental equation is sometimes required, except for the simplest type of dispersion. The price to be paid is, as in most examples of nonlinear equations that can be solved in a relatively easy manner, that this example is of little practical importance. Its significance still is based on showing the emergence of new phenomena that can guide more complicated examples.

Let us briefly consider the simplest possible example of factorization of the ω dependence in $M_{ij}(\vec{k},\omega)$ without going into the details. Let us suppose we form a PDS out of two different materials with optical constants $\epsilon_a(\omega)$ and $\epsilon_b(\omega)$. We assume that both dielectric objects and background have *the same* gap ω_0 but different oscillator strengths. We further take one example that does not require numerical handling of the roots. We assume both $\epsilon_{a,b}(\omega)$ to be given by the two-level system expressions

$$\epsilon_{a,b}(\omega)\sim\epsilon_{a,b}(\infty)+\frac{[\epsilon_{a,b}(0)-\epsilon_{a,b}(\infty)]}{1-\omega/\omega_0}. \tag{7}$$

In this way, the problem can be solved by working out the roots of the *dispersionless* problem (2–3) with $[\epsilon_{a,b}(0)-\epsilon_{a,b}(\infty)]$ in (6) and transforming the spectrum of eigenvalues by

$$\omega'\rightarrow-\frac{\omega^2}{2\omega_0}+\sqrt{\frac{\omega^4}{4\omega_0^2}+\omega^2}. \tag{8}$$

The transformation (8) is valid only for those roots ω of the spectrum for which (7) holds, in practical terms, for $\omega<\omega_0$, but sufficiently close to resonance so that we can neglect the $\omega\rightarrow\infty$ limit of $\epsilon(\omega)$. Besides modifications in the gaps, Eq. (8) induces a quadratic $\vec{k}$ dependence in the dispersion for ω' (in a somewhat similar fashion as the nonparabolicity of electron bands) and a substantial diminution (depending on ω_0) of the group velocity in the *acoustic branches*. Had we selected a different type of singularity for the dispersion of $\epsilon_{a,b}(\omega)$ then, the transformation of the spectrum of eigenvalues has to be performed numerically from an implicit equation of the form $F(\omega',\omega)=0$. Equation (7) has been deliberately chosen because it allows an explicit expression for ω' as a function of the roots of the dispersionless problem ω.

VI. ACOUSTIC BRANCHES AND LONG-WAVELENGTH EFFECTIVE MEDIUM

It is well known from the theory of acoustic phonons that the long-wavelength limit can be treated as continuum problem which ignores the microscopic structure of the lattice. In terms of the elastic constants $c_{\mu\sigma\nu\tau}$ the acoustic modes are solutions of $\rho\omega^2 a_\mu=c_{\mu\sigma\nu\tau}k_\sigma k_\nu a_\tau$, where ρ is the density and $\vec{a}$ the polarization vector.[31] The harmonic potential for the continuum reads $U=1/2e_\alpha C_{\alpha\beta}e_\beta$ with e_α being the strain components and $C_{\alpha\beta}$ the elastic stiffness constants. For a given $\vec{k}$ there are three eigenvalues and their corresponding eigenvectors $\vec{a}$. These are *exactly* longitudinal or transverse to $\vec{k}$ only along high symmetry directions. If we assume the lattice at rest and we force a given amplitude for the strain e_μ components representing a mode, we have to invest some energy according to the polarization selected. The larger the energy the more *rigid* the medium and the faster the speed of sound for that polarization.

Suppose we want to force upon a PDS a low-frequency $\omega\rightarrow0$ field with a given polarization. We can control the electric displacement $\vec{D}$ from the outside (we only have ac-

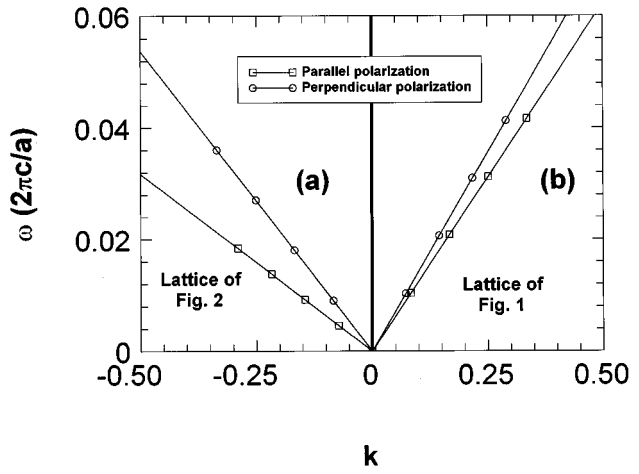

FIG. 11. Long-wavelength acoustic branches for both polarizations. (a) branches for the lattice of Fig. 2. (b) same for the lattice of Fig. 1. Note that electromagnetic waves always travel faster for $\perp$ polarization in these structures, reflecting the fact that $\epsilon_{\perp} < \epsilon_{\parallel}$. The result is also valid for PDS's made of air rods in a dielectric medium. The slopes of the branches obtained in the calculations are expected to satisfy the proportionality $v \sim 1/\sqrt{\epsilon_{\text{effective}}}$ and can give accurate values of the *effective dielectric components* of the structure for static fields. The inverse of the dielectric tensor componets play the role of the elastic stiffness constants in the analogy with classical acoustic waves.

cess to the free charges, while $\vec{E}$ is fixed by the the external field and the internal rearrangement of charges). Suppose, for example, we have two parallel plates with equal positive and negative charges, respectively, and we want to introduce these plates inside the PDS with a given orientation (parallel or perpendicular to the rods). There is an energy associated with this configuration given by $U = 1/2[1/\epsilon_{ij}(0)]D_i D_j$ for a fixed $\vec{D}$. The smaller the *effective dielectric function* for a given polarization the larger the energy. This a measure of the rigidity of the mode and the smaller the ϵ the faster the mode for that polarization. This is the reason why all PDS's in 2D have always the acoustic branches $\perp$ to the rods faster than those $\parallel$ since the effective dielectric constants normally satisfy $\epsilon_{\perp} < \epsilon_{\parallel}$. In Fig. 11 we show the long wavelength acoustic branches for both polarizations and for both examples given in Figs. 1 and 2. In the analogy with acoustic waves, the inverse of the dielectric tensor plays the role of the elastic stiffness constants for acoustic phonons. Analogies of this type are not surprising since mechanical and electromagnetic systems are known to have equivalences; the typical example being the damped oscillator and a LRC circuit. The important point to recognize here is, however, that long-wavelength acoustic branches have information on the average properties of the medium treated as a continuum and the equivalent branches in PDS's can be used to obtain information on the *effective dielectric properties* of the structure. Following Refs. 7 and 32, an estimation of the effective long-wavelength dielectric constants for a given structure can always be obtained from the limiting cases of maximum ($\vec{E}\parallel$ to all interfaces) and minimum ($\vec{E}\perp$ to all interfaces) screening given by

$$\epsilon = f\epsilon_a + (1-f)\epsilon_b \tag{9}$$

and

$$1/\epsilon = f/\epsilon_a + (1-f)/\epsilon_b, \tag{10}$$

respectively. These formulas are not strictly correct because they neglect the real field distribution at the boundaries of the rods, but give the appropriate order of magnitude. In the example of Fig. 11(a) they predict a ratio of speeds for the two polarizations given by $v_{\perp}/v_{\parallel} \sim 0.502$, while the calculated ratio is 0.587. For Fig. 11(b) we obtain $v_{\perp}/v_{\parallel} \sim 0.831$ to be compared with the calculated one of 0.873. These speeds are, of course, independent of the direction chosen for $\vec{k}$ in the limit $\vec{k} \to 0$ as can be checked from the acoustic branches in Figs. 1 and 2. The small corrections to the result given by (9–10) arise from the actual details of the field distributions of the modes for different polarizations around the dielectric objects forming the lattice, and produce the same quantitative result one would get by solving the *electrostatic* problem and evaluating the effective screening for a given electric field. These corrections depend, of course, not only on the dielectric functions of the rods and background as in (9–10) but also on the selected type of lattice and rods.

VII. CONCLUSIONS

We have exploited several analogies with phonons and electrons to highlight different aspects of the electromagnetic excitations in periodic dielectric structures. A detailed account of electromagnetic surface states obtained from the bulk band structure and emission produced by a point source with all its consequences of focusing and internal diffraction has not been given before to the best of our knowledge. In addition, we discussed briefly the possibility of including dispersion in the dielectrics and show that this particular aspect has no direct analog for electrons. The simplest possible example of this type has been discussed. Further work on the latter is under way and will be published elsewhere.[33] A few analogies with the elastic theory of acoustic phonons and the link with the electrostatics of the problem and the *effective-medium dielectric properties* have been highlighted in the last section. We confronted the different analogies from a solid-state physicist's point of view and emphasized simple concepts rather than mathematical or computational complexity.

ACKNOWLEDGMENTS

Special thanks are given to A. Fainstein (CNET-Telecom, France) for a critical reading of the manuscript as well as for interesting comments and suggestions. It is a pleasure also to thank N. Garro-Martinez and A. Cantarero (University of Valencia) for useful comments. Pablo Etchegoin wishes to thank the European Union for financial support in Cambridge (UK). This work was supported by EPSRC (UK).

[1] E. Yablonovitch, Phys. Rev. Lett. **58**, 2059 (1987).
[2] S. John, Phys. Rev. Lett. **58**, 2486 (1987).
[3] K. M. Ho, C. T. Chan, and C. M. Soukoulis, Phys. Rev. Lett. **65**, 3152 (1990).
[4] M. Plihal and A. A. Maraudin, Phys. Rev. B **44**, 8565 (1991); M. Plihal, A. Shambrook, A. A. Maraudin, and P. Sheng, Opt. Commun. **80**, 199 (1991).
[5] P. R. Villeneuve and M. Piché, Phys. Rev. B **46**, 4973 (1992).
[6] E. Yablonovitch, T. J. Gmitter, and K. M. Leung, Phys. Rev. Lett. **67**, 2295 (1991); J. Opt. Soc. Am. A **7**, 1792 (1990); E. Yablonovitch, T. J. Gmitter, and R. Bhat, Phys. Rev. Lett. **61**, 2546 (1988).
[7] W. M. Robertson, G. Arjavalingam, R. D. Meade, K. D. Brommer, A. M. Rape, and J. D. Joannopoulos, Phys. Rev. Lett. **68**, 2023 (1992).
[8] See, for example, J. Opt. Soc. Am. B **10**(2), 280 (1993), and references therein. See, also, *Confined Electrons and Photons*, edited by E. Burstein and C. Weisbuch (Plenum, New York, 1995).
[9] S. John, Phys. Rev. Lett. **53**, 2169 (1984); Phys. Today **44** (5), 32 (1991).
[10] I. Freund, M. Rosenbluh, R. Berkovits, and M. Kaveh, Phys. Rev. Lett. **61**, 1214 (1988).
[11] A. Z. Genack, Phys. Rev. Lett. **58**, 2043 (1987).
[12] M. Drake and A. Z. Genack, Phys. Rev. Lett. **63**, 259 (1989).
[13] E. Akkermans, P. E. Wolf, R. Maynard, Phys. Rev. Lett. **56**, 1471 (1986).
[14] *Scattering and Localization of Classical Waves in Random Media*, edited by P. Sheng (World Scientific, Singapore, 1990).
[15] E. Yablonovitch, J. Opt. Soc. Am. B **10**(2), 283 (1993).
[16] H. De Raedt, A. Lagendijk, and P. de Vries, Phys. Rev. Lett. **62**, 47 (1989).
[17] R. D. Meade, K. D. Brommer, A. M. Rappe, and J. D. Joannopoulos, Phys. Rev. B **44**, 10 961 (1991).
[18] M. L. Cohen and T. K. Bergstresser, Phys. Rev. **141**, 789 (1966).
[19] E. T. Goodwin, Proc. Cambridge Philos. Soc. **35**, 205 (1935).
[20] C. M. Chaves, N. Majlis, and M. Cardona, Solid State Commun. **4**, 271 (1966); **4**, 631 (1966).
[21] P. Yeh, A. Yariv, and A. Cho, Appl. Phys. Lett. **32**, 104 (78).
[22] W. Ng, P. Yeh, P. C. Chen, and A. Yariv, Appl. Phys. Lett. **32**, 370 (78).
[23] A. A. Bulgakov and V. R. Kovtun, Opt. Spectrosc. (USSR) **56**, 471 (84).
[24] A. A. Bulgakov and K. R. Kovtun, Solid State Commun. **56**, 781 (85).
[25] S. D. Gupta and B. Buti, Indian J. Pure Appl. Phys. **23**, 452 (85).
[26] R. D. Meade, K. Brommer, A. M. Rappe, and J. D. Joannopoulos, Phys. Rev. B **44**, 13 772 (1991); Phillip St. J. Russell, Thimothy A. Birks and F. Dominic Lloyd-Lucas in *Confined Electrons and Photons*, edited by E. Burstein and C. Weisbuch (Plenum, New York, 1995), p. 585.
[27] A. Yariv and P. Yeh, *Optical Waves in Crystals* (Wiley, New York, 1983), p. 79.
[28] G. A. Northrop and J. P. Wolfe, Phys. Rev. Lett. **43**, 1424 (1979); Phys. Rev. B **22**, 6196 (1980); R. Eichele, R. P. Huebener, and H. Seifert and K. Seilig, Phys. Lett. **87A**, 469 (1982); R. Eichele, R. P. Huebener, H. Seifert, Z. Phys. B **48**, 89 (1992).
[29] H. J. Maris, Phys. Rev. B **28**, 7033 (1983).
[30] J. P. Wolfe, Phys. Today **48**(9), 34 (1995).
[31] A. E. H. Love, *A Treatise on the Mathematical Theory of Elasticity* (Dover, New York, 1944).
[32] D. E. Aspnes, Am. J. Phys. **50**, 704 (1982).
[33] P. Etchegoin and R. T. Phillips (unpublished).